Available online at www.sciencedirect.com
SCIENCE DIRECT®
Earth and Planetary Science Letters 239 (2005) 219–232
EPSL
www.elsevier.com/locate/epsl

Giant meteoroid impacts can cause volcanism

Linda T. Elkins-Tanton [a,*], Bradford H. Hager [b,1]

[a] Brown University, Department of Geological Sciences, 324 Brook Street, Providence, RI 02912, USA
[b] Massachusetts Institute of Technology, Department of Earth, Atmospheric and Planetary Sciences, Cambridge, MA 02139, USA

Received 20 November 2004; received in revised form 26 July 2005; accepted 29 July 2005
Available online 13 October 2005
Editor: S. King

Abstract

We present a model to assess the viability of the creation of volcanic eruptions of up to flood-basalt size from a giant impactor striking a relatively thin lithosphere. A 300-km-radius crater in 75-km-thick lithosphere can create 10^6 km^3 of magma from instantaneous in situ decompression of mantle material with a potential temperature of 1300 °C. For a range of lithospheric thicknesses and potential temperatures, subsequent adiabatic melting caused by mantle convection beneath the lithosphere at the site of the impact can create additional magma. Though the evidence that a giant impactor has struck at the location of any terrestrial flood-basalt province is equivocal, there are possible age coincidences between evidence for impacts and occurrences of flood basalts. Our model demonstrates that a giant impactor could cause a flood basalt, and this process may have been significant early in Earth history when impactors were more frequent and mantle temperatures likely higher, though other processes are required for at least the majority of flood-basalt provinces today.
© 2005 Elsevier B.V. All rights reserved.

Keywords: impact; volcanism; flood basalt; mantle melt; extinction

1. Introduction

Since the suggestions of Alvarez et al. [1] that an extraterrestrial impact caused the extinction at the Cretaceous–Tertiary boundary, researchers have been searching for evidence of impacts coincident with extinctions, and increasing numbers of horizons with elevated iridium, shocked quartz, and other indicators have been found. An apparent coincidence of ages between several flood-basalt events and several extinctions is also reported (e.g., [2]), and the idea that giant crater-forming impact can cause volcanic activity at the site of impact has been proposed by a number of researchers (e.g., [3–12]), and opposed by others (e.g., [13,14]).

There is some evidence for a crater underneath or close to the Deccan flood basalts themselves [10,15]. Becker et al. [16] reported evidence for a large impact at the time of the Siberian flood basalts based on trapped helium and argon in fullerines, but the finding is controversial and remains to be replicated by another laboratory. Xu et al. [17] report high iridium concentration at the Permian boundary, but this measurement is strongly contested by Orth et al. [18]. Kaihu et al. [11] report a large sulfur and strontium excursion and impact-metamorphosed mineral grains coincident with the end Permian. They interpret these findings as indicative of a 30–60-km asteroid strike, creating a crater with a radius from 300 to 600 km.

* Corresponding author. Tel.: +1 401 863 3185.
E-mail addresses: Linda_Elkins_Tanton@brown.edu (L.T. Elkins-Tanton), bhhager@mit.edu (B.H. Hager).
[1] Tel.: +1 617 253 0126.

0012-821X/$ - see front matter © 2005 Elsevier B.V. All rights reserved.
doi:10.1016/j.epsl.2005.07.029

There is a report of shocked minerals at 200 Ma [19], the time of the Central Atlantic Magmatic Province. Rampino and Haggerty [20] report evidence for high iridium levels at 200 Ma. Despite these intriguing reports, unequivocal evidence for simultaneous occurrences of giant impacts and flood basalts has not been found on Earth.

We describe here a mechanism for the formation of volumes of magma equivalent to flood basalts by a giant impact on thin continental lithosphere over a fertile mantle with potential temperature between 1250 and 1450 °C. Magma can be produced in two stages. First, crater excavation may depressurize underlying material such that it melts in situ. Second, the cratered lithosphere may rise isostatically, warping isotherms at the lithosphere–asthenosphere boundary and initiating convection, in which adiabatic melting can occur (Fig. 1). This model is similar to a model for impact-produced volcanism on the Earth proposed by Jones et al. [7], though that model includes only the depressurization from excavation, and no later convection. Ivanov and Melosh [14] have stated that impacts cannot initiate volcanic eruptions, though their model predicts the creation of 2×10^4 km^3 of magma from a crater with radius 100–150 km, in lithosphere 60–70 km thick, with an underlying mantle potential temperature of about 1230 °C. This is very close to our own result. We use, however, higher temperatures and larger impacts, which necessarily create more melt. The radii of excavation of the final crater in the numerical experiments presented here are 50 km or larger.

Craters of this size have been estimated to occur at a rate of ~10–50 per billion yr [13,14,20,21]. To form a significant volcanic province according to this model, the impact must occur in relatively thin lithosphere and avoid deep ocean waters, thus limiting the area of potential targets on Earth. We suggest that this process was more pertinent early in Earth's history, when giant

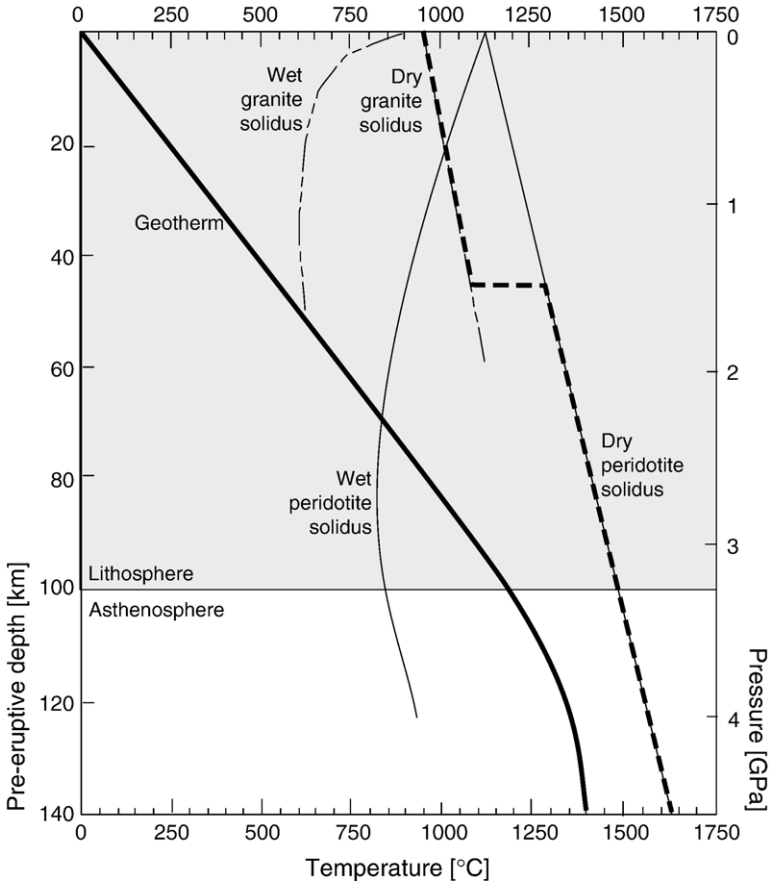

Fig. 1. Thermal and compositional model used in melt volume calculations for both in situ decompression and convective melting. Dashed and dotted lines: wet and dry granite solidii; solid lines: wet and dry peridotite solidii. Bold lines mark the modeled solidus and initial geotherm. Lithospheric thicknesses of 50–150 km are also used, with mantle potential temperatures of 1250, 1300, 1350, and 1450 °C.

basin-forming impacts were more common and the mantle probably hotter.

2. Models

There are three stages in the impact process that can create melt: (1) Initial impact causes shock melt; (2) excavation of material from the impact site can cause instantaneous decompression melting beneath the impact site; and (3) development of a dome in the lithosphere–asthenosphere boundary, either through instantaneous liquid flow of the shocked lithosphere or through later isostatic rebound, induces convection due to the horizontal temperature gradient at the edges of the dome, and upwelling mantle material in these convective cells can, under some circumstances, melt adiabatically (see Fig. 1 in [6]).

2.1. Constraints on lithospheric thickness and mantle temperature

As in any model addressing flood basalts, bringing the required volume of mantle material above its solidus is at the heart of the problem. The higher the mantle potential temperature, the deeper mantle melting can begin, and the larger the resulting melt fraction and volume of magma. Similarly, if the lithosphere is thin, asthenospheric material can be decompressed to lower pressures and more easily melt. We define the lithosphere as material cooler than 1000 °C and the asthenosphere as all underlying material. We model craters with excavation radii from 50 to 300 km in lithospheres from 40 to 150 km thick. We do not model any impacts that would completely remove the lithosphere. Though the results of such an impact would no doubt be catastrophic, they would not necessarily follow the process we are modeling.

These models do not rely on unusual asthenospheric temperatures to allow melting. Plank and Langmuir [22] estimated that the potential temperature under mid-ocean ridges ranges from 1260 to 1510 °C, and Kinzler and Grove [23] estimated a range of 1290–1435 °C. Though Presnall et al. [24] estimated 1240–1260 °C, Green et al. [25] estimated 1430 °C for both MORBS and hot spots. Based on this petrologic data and modeling, mantle potential temperatures from 1240 to 1430 °C might be considered reasonable for the modern mantle, and those at the high end perhaps more pertinent for the Archean mantle. For a 50-km-thick lithosphere, melt exists in the mantle below it for potential temperatures greater than about 1250 °C. We therefore suggest that using an asthenospheric potential temperature higher than 1250 °C under a lithosphere 50 km thick is unrealistic if there was no previous evidence for magmatic activity at the site of impact (though it has been suggested that some amount of melt exists in the upper mantle at all times; see [26]). Though melt volumes are calculated for mantle potential temperatures where there would be existing melt, they are denoted as such in tables and figures and are presented as an interesting extension of the theory and not as a generally plausible condition. Mantle potential temperatures of 1250, 1300, 1350, and 1450 °C are used. See Fig. 1 for the initial lithospheric and asthenospheric model used in this study. Note also that the dry peridotite solidus used in these idealized models will create a minimum melt volume when compared to melting of hydrated or eclogite-rich mantle materials.

2.2. Crater models

The evolution of the shape of craters, from the first seconds after impact through isostatic rebound perhaps thousands of years after impact, is controversial. Because material excavated from the crater is thrown farther than any possible radius of inward flow, thinning of the lithosphere and depressurization of the underlying mantle will result regardless of the magnitude of lateral crater collapse. This simple assumption removes some of the controversy over the possibility of instantaneous lateral resurge filling the crater and disallowing in situ melting; if the mass has been ejected from the crater, then a mass deficiency exists for the lithosphere in the region of the crater, and our modeled processes will proceed.

The removal of ejecta might not be as effective in the case of an oceanic impact. The rapid resurge of a wall of water back into the crater, perhaps carrying with it sediment and breccia, is likely to largely refill the crater and decrease the amount of depressurization. It is thought that this process rapidly refilled Chicxulub [27].

The crater models considered are based on the models of O'Keefe and Ahrens [28,29] and Cintala and Grieve [30]; see Fig. 2. The maximum depth of excavation equals $0.15R$, where R is the radius of excavation (melt production for an excavation depth of $0.10R$ is also calculated). The value $0.15R$ is also the maximum isostatic uplift of the bottom of the lithosphere under the crater. The radius of the final crater, including outer ring structures, is about $1.9R$.

The complex terrestrial crater depth profile (D_C) of O'Keefe and Ahrens [29] is closely fitted by the following expression, where R is the radius of excavation

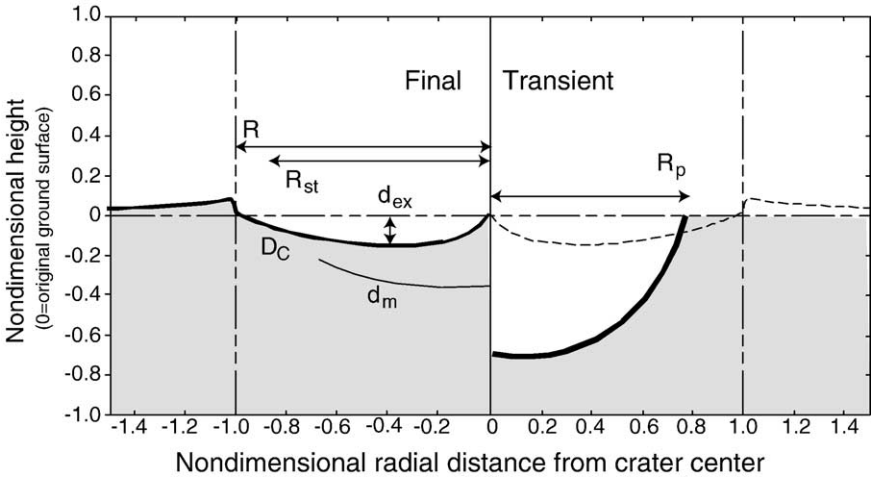

Fig. 2. Model of crater profiles used in melt modeling, showing the radius of excavation, R, the radius at which stratigraphy is turned 90° (R_{st}), the radius of impactor penetration (R_p), the depth of excavation (d_{ex}), and the depth of melting (d_m). Adapted from [28–30]. D_C, the crater profile given by Eq. (1), is shown in the bold line on the left side of the diagram.

of the crater, and r is radial distance from the center of the crater, all in kilometers:

$$D_C = R\left(\frac{0.2r^3}{R^3} + \frac{0.022}{\frac{r}{R}+0.1} - 0.22\right) \quad (1)$$

When integrated, this profile yields the following expression for excavated crater volume, V:

$$V_C = 0.11\pi R^3 \quad (2)$$

This excavated volume is matched to the total ejecta volume obtained by integrating the following expression for ejecta blanket thickness, D_E, as a function of distance from the crater's outer edge:

$$D_E = \frac{0.34R^4}{r^3}. \quad (3)$$

The crater depth profile is used in both the in situ decompression melting model and the model of the formation of the lithospheric dome for subsequent convective melting.

The resulting volumes are in agreement with the ejecta law given in Housen et al. [31], and crater profiles are roughly in agreement with those given in Melosh [32] and Grieve and Cintala [33].

2.3. Impactor size and energy

Assuming that impacts excavate 100 times their own mass (e.g., [32]), the average upper lithospheric density is 2500 kg/m^3, and the volume of the initial crater is given as Eq. (2), the mass and, therefore, radius of impactor required to create the modeled craters can be calculated. To create a crater with a 50-km radius, depending on the density and speed of the impactor, an impactor with radius of 3–5 km is required. To create a crater with 300-km radius, an impactor with 15–25-km radius is required.

Modeling impact energy simply as $mv^2/2$ (where m = impactor mass and v = impactor velocity) and assuming impactors will strike at between 10 and 40 km/s [34], the energy of impact for the modeled craters varies between 10^7 and 10^{10} Mt (10^{22}–10^{26} J). A range of estimates of impact rates suggest that impacts of this size should occur between 10 and 50 times per billion yr, suggesting that 5–25 such events should exist in the Phanerozoic record [14,21], with 2–8 on continents.

2.4. Modeling melt volumes

2.4.1. Shock melt from impact

The first stage of melting, shock melting from the energy of impact, was not modeled here. A 300-km-radius crater makes about 10^5 km^3 of shock melt, and a 100-km-radius crater about 10^4 km^3 of melt, in each case between 10% and 1% of the volume required to make a flood-basalt province [35,36]. Because the crust is compositionally distinct from the mantle, shock melts are generally compositionally distinct from adiabatic mantle melts, would not be mistaken for them, and so are not included in this study.

2.4.2. Stage 1: in situ decompression melting

At the time when impact material at the impact site is ejected, and within a certain additional radius, material is melted (shock melt) or disrupted and heated by

shock. In giant craters, the volume of material heated but not melted may be considerable, but this heating process is not considered in this model. Energy partitioning from the impact among heating the lithosphere, heating the atmosphere, excavating lithospheric material, and compressing lithospheric material is not well constrained. Were lithospheric heating included, in situ melt volumes might be higher and asthenospheric convection might be more vigorous. For simplicity, a conductive geotherm through the lithosphere culminating at a boundary layer with an adiabatic asthenosphere is assumed to remain in place after excavation.

Excavation of the crater reduces pressure beneath the crater by an amount equal to the lithostatic pressure of the material excavated. The greatest pressure release is over the interval from 20% to 40% of the radius of excavation, and pressure release declines to zero at the crater rim (and can increase outside the rim due to new deposits). This lowering of pressure effectively moves the solidus deeper into the material, in some cases causing it to cross the geotherm and create melt. This melting mechanism is shown in the detail of Fig. 1 of Elkins-Tanton et al. [6]. A general equation for in situ decompression melt was created by integrating the area of intersection between the solidus and geotherm around the axis of symmetry of the crater. The parameters used in the equations are given in Table 1.

A critical parameter is β, the melt fraction per degree between solidus and liquidus. This can be calculated using C_p, the heat capacity of the silicates, and H_f, the heat of fusion of the silicates, as follows:

$$\beta = \frac{df}{dT} = \frac{C_p}{H_f} = 0.3\,\frac{\text{wt.\%}}{^\circ} \tag{4}$$

Based on this df/dT and the maximum decompression created by any impact modeling, the maximum melt percent of a parcel of mantle in the in situ melting model is 15%. In fertile mantle peridotite, melting about 20% is generally required to exhaust clinopyroxene and change the melting productivity [23,37]. Thus, a constant df/dT is a reasonable assumption.

The geotherm is initially modeled as a straight, conductive profile through the lithosphere from the surface to the adiabatic potential temperature at the base of the lithosphere and as an adiabat through the mantle. The solidus is approximately that of Hirschmann [38]. The following expressions describe the geotherm in the lithosphere, which is conductive, and in the mantle, where it is adiabatic:

Lithospheric geotherm:

$$T_A = z\left(\frac{T_p}{d} + a\right) \tag{5}$$

Table 1
Parameters used in melt volume calculations

Constants used in melt volume calculations		
s	slope of solidus	3.0 °/km
h_o	maximum crater excavation depth=0.15R	km
R	radius of excavation of the crater	50, 100, 200, 300, 400 km
s_o	solidus temperature at 1 atmosphere	1120 °C
T_p	mantle potential temperature	1250, 1300, 1350, or 1450 °C
d	lithospheric thickness	50, 60, 70, 100, and 150 km
a	slope of the adiabat	0.33 °/km
C_P	heat capacity of silicates	1256.1 J/°kg
H_f	heat of fusion of silicates	418,700 J/kg
β	fraction of melt produced per degree above solidus	0.003 df/dT
Variables used in in situ melt volume calculations		
z	depth, 0 at original land surface	km
r	radial distance from crater center	km
$D_C(r)$	crater excavation depth	km
$T_A(z)$	geotherm in the lithosphere	°
$T_B(z)$	geotherm in mantle	°
$T_C(z)$	solidus after crater excavation	°
z_u	where T_A and T_C cross: shallowest limit of melt	km
z_l	where T_B and T_C cross: deepest limit of melt	km
F	volume of melt	km^3
Constants used in numerical modeling of convection		
h	height and width of model box	500 km
ρ	reference mantle density	3300 kg/m^3
g	gravitational acceleration	9.8 m/s^2
ΔT	temperature across the model box	1250, 1300, 1350 or 1450 °C
η_o	reference viscosity	10^{18}–5×10^{20} Pa s
α	thermal expansivity	$3\times10^{-5}/^\circ$
σ_o	reference stress	1.6×10^{13} Pa
κ	thermal diffusivity	10^{-6} m^2/s
e	number of elements in model box, each dimension	120
Ra	Rayleigh number	1.5×10^6

Mantle geotherm (adiabatic):

$$T_B = az + T_p. \tag{6}$$

A solidus for mantle material can be expressed as follows, and subsequently as it appears following excavation of the crater:

Solidus:

$$T_S = sz + s_o \tag{7}$$

Solidus following crater excavation:

$$T_C = s(z + D_C) + s_o \tag{8}$$

where the expression for the crater profile, D_C, is given by Eq. (1) above.

The integration is performed in two parts, one from the intersection of the solidus and the adiabat (z_l, where equation T_B equals equation T_C) upward to the base of the lithosphere (where the geotherm changes slope and becomes conductive), and the second from the base of the lithosphere to the intersection between the solidus and the conductive geotherm (z_u, where equation T_A equals equation T_C). The maximum temperature interval for melting between the solidus and geotherm is found over the interval from 0.2 to 0.4 of the radius of excavation. As the radius increases toward the edge of the crater, the solidus effectively moves upward, following the crater floor, and the melting interval decreases (Fig. 2). The final equation for in situ melt is given as

$$F = 2\pi\beta\left[\int_{d}^{z_l}\int_{0}^{R} r(T_B - T_C)\mathrm{d}r\mathrm{d}z + \int_{z_u}^{d}\int_{0}^{R} r(T_A - T_C)\mathrm{d}r\mathrm{d}z\right] \quad (9)$$

This equation for F is easily integrated, and the result is an equation for in situ melt as a function of R, d, s, a, s_o, and T_p.

Because silicic crustal materials have, in general, a lower temperature solidus than do mafic mantle materials, it is tempting to use their solidus in calculating intersections with the geotherm in the lithosphere. If a great percentage of the lithosphere is made up of silicic materials, it is possible to melt crustal materials through in situ depressurization. This process may be important in the formation of ore bodies such as Sudbury, but crustal melting is not modeled in this paper.

2.4.3. Stage 3: adiabatic melting in convection currents

The excavated crater profile shown on the left side of Fig. 2 is not in isostatic equilibrium; the thinned lithosphere will rise and form a dome, both at the surface and at the lithosphere–mantle boundary. The process of forming a dome may occur virtually instantaneously, when the lithosphere behaves as a liquid due to the intense shock of the impact. Alternatively, the lithosphere may rebound isostatically over approximately the next 10^4 yr, on a time scale similar to that predicted for post-glacial rebound on Earth [39].

Domes under lunar impact basins have been clearly identified by lunar gravity modeling [40,41], but they have not been demonstrated on Earth. Comparisons between lunar and terrestrial lithospheric rebound are complicated by a lack of physical constraints on the lunar Nectarian and Pre-Nectarian lithosphere, though higher internal temperatures in the early evolution of both bodies would have enhanced rebound. There are a number of possible reasons for the lack of evidence for terrestrial lithospheric domes. First, the smallest lunar basins that show domes are about the size of the very largest terrestrial impacts yet recognized. On the moon, domes are present for basins that range in size from Imbrium to Smythii. Imbrium has a radius of excavation of about 350 km and Smythii about 80 km; Chicxulub, on Earth, had an excavation radius of about 50 km [40–43]. If domes are formed by instantaneous fluid flow of shocked lithosphere, then it is possible that the process requires basin-forming impacts larger than that of Chicxulub. Alternatively, domes may have formed in the largest terrestrial impacts but were obliterated by later processes. Buoyant residuum from in situ melt would fill the lithospheric dome and end convective melting. The buoyant residuum, combined with possible long-term lateral middle-crustal flow and cooling and thickening of the lithosphere, could obscure any original lithospheric dome from detection by seismic surveys.

We suggest that terrestrial lithospheric domes will form by nearly instantaneous flow combined with later isostatic compensation for giant impacts in thin lithospheres. All the impacts modeled in this study (with the exception of the 50 km-radius crater in 150-km-thick lithosphere) penetrate or disrupt, through shock, the entire thickness of the lithosphere. Therefore, all the impacts modeled are expected to create significant lithospheric flow and create at least a partial lithospheric dome. Based on analysis of the shape and size of the central uplift feature in the Vredefort impact structure, Henkel and Reimold [44] calculated that the viscosity of the crust during initial deformation was about 10^{12} Pa s. This viscosity is orders of magnitude less than normal asthenospheric and crustal viscosities. This low viscosity is strong support for immense volumes of rock involved in liquid flow at the time of giant impact. Later, as the in situ decompression melts erupt, the thinned, weakened lithosphere may subside. This would be consistent with the critical geological observation that the surface under both the Siberian and the Emeishan basalts were subsiding while the basalts were erupting [45,46].

When the lithospheric dome forms, it necessarily results in a horizontal temperature gradient across its edges, which provides a driving force for convection. Adiabatic melting may occur in the resulting convective cells, depending on the depth and temperature of the mobilized mantle materials. This third melting stage begins as soon as immediately after impact and, at latest, on the order of 10^4 yr after impact.

The convection is calculated numerically using a spherical axisymmetric version of the finite element code ConMan [47], called SSAXC, and the resulting melt is calculated with a post-processor routine using the parameters listed in Table 1. We ran a large suite of test models to ensure that the code was correctly calculating the convective flow and to ensure that the grid had sufficient resolution to avoid numerical artifacts.

The Rayleigh number governs thermal convection:

$$Ra = \frac{\rho g \alpha \Delta T h^3}{\eta_o \kappa} \tag{10}$$

where α is thermal expansivity, κ is thermal diffusivity, ρ is a characteristic density, ΔT is the temperature change over the model box, h is a characteristic length and η_o is a reference viscosity. Viscosity is calculated using the following non-Newtonian law:

$$\eta_{\text{nonN.}} = \eta_o \left(\frac{\sigma_o}{\sigma}\right)^2 \exp\left(\frac{E + vz}{T + T_o} - \frac{E + vz_o}{1 + T_o}\right) \tag{11}$$

where η_o, σ_o, z_o, and T_o are reference values for viscosity, stress, depth, and temperature, respectively; E is the activation energy, and v is the activation volume. With this stress dependence, a factor of 2.2 in deviatoric stress, σ, creates a factor of 10 change in strain rate. The use of a stress-dependent law is appropriate for materials deforming by dislocation creep, as material at asthenospheric temperatures and viscosities undergoing convective stress is likely to be. A list of key variables is given in Table 1.

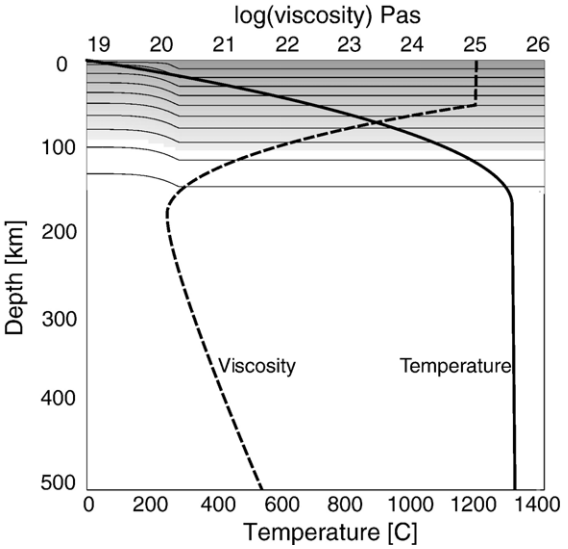

Fig. 3. Starting conditions (redimensionalized) for a numerical experiment with lithospheric depth of 100 km and rebounded crater with excavation radius 200 km. Thin solid lines are isotherms, also shown by shading. Viscosity is shown with the dashed line and top axis and temperature with the thick solid line and bottom axis.

A starting condition for each model run was created by using a complementary error function cooling law to make a cooled lithosphere of the desired depth. The lithosphere–asthenosphere boundary is given a dome with maximum uplift equal to 0.15 times the crater excavation radius, employing the temperature at the surface (T_S), the temperature of the convecting mantle (T_M), thermal diffusivity (κ), and the time period of thermal diffusion (τ) [48]:

$$T(z) = (T_S - T_M)\text{erf}c\left[\frac{z}{2(\kappa\tau)^{0.5}}\right] + T_M. \tag{12}$$

An example set of starting conditions for the numerical experiments is shown in Fig. 3.

3. Results

3.1. Stage 1: in situ decompression melting

In situ decompression melt is the largest and, for most parameters, the only contributor to melt created by giant terrestrial impacts. Table 2 lists the total melt produced in the model, and Fig. 4 shows the variation in total melt volume with crater radius, lithospheric thickness, and mantle potential temperature. Volumes of melt consistent with flood-basalt provinces are created by large impacts in thin lithospheres, without resorting to mantle potential temperatures that would create extant melt before impact. The impact-generated mafic mantle melts originate at depths from the lowest part of the lithosphere to as much as 175 km. The maximum depth of the melting interval is also listed in Table 2. This depth of melting is unusual for terrestrial processes; melting in mid-ocean ridge environments, for example, begins shallower than about 50 km.

Lithospheric thickness, mantle potential temperature, and crater excavation depth are all controlling parameters in impact melt generation. Table 3 shows the effects of these three parameters on melt generation. At a constant mantle potential temperature and excavation depth, increasing lithospheric thickness by 10 km reduces melt volume by between 20% and 40%, depending upon crater radius. Increasing mantle potential temperature by 50 °C, holding other parameters constant, increases melt volume by a factor of 2 or 3. Finally, decreasing crater excavation depth from $0.15R$ to $0.10R$ reduces melt production by about 50%.

Table 2
Melt volume totals for all stages of melt production

Lithosphere thickness (d) (km)	Crater radius (r_o) (km)	T_p 1250	h_o 0.15	η_o 10^{20}
		In situ melt volume (km^3)	Maximum melt depth (km)	Total melt volume (km^3)
50	50	3.6×10^3	55	3.6×10^3
	100	2.6×10^4	63	2.6×10^4
	200	3.9×10^5	80	3.9×10^5
	300	2.1×10^6	96	2.1×10^6
70	200	1.5×10^5	80	1.5×10^5
	300	7.8×10^5	96	7.8×10^5
100	400	2.2×10^6	113	2.2×10^6
150	400	0		0

Lithosphere thickness (d) (km)	Crater radius (r_o) (km)	T_p 1350	h_o 0.15	η_o 10^{19}	Convective melt volume (km^3)	Convective melt duration (Ma)	Total melt volume (km^3)
		In situ melt volume (km^3)	Extant melt fraction	Maximum melt depth (km)			
50	50	2.0×10^4	0.62	86	0	0	5.2×10^4
	100	1.6×10^5	0.45	95	0	0	2.9×10^5
	200	1.5×10^6	0.26	111	2.0×10^4	0	2.0×10^6
	300	5.8×10^6	0.17	127	2.6×10^4	5	7.0×10^6
70	50	9.3×10^3	0	86	0	0	9.3×10^3
	100	7.6×10^4	0	95	0	0	7.6×10^4
	200	8.2×10^5	0	111	4.4×10^3	5.5	8.2×10^5
	300	3.6×10^6	0	127	2.1×10^4	5	3.6×10^6
100	200	1.7×10^5	0	111	0	0	1.7×10^5
	300	9.1×10^5	0	127	0	0	9.1×10^5
	400	3.7×10^6	0	144	0	0	3.7×10^6
150	400	0	0		0	0	0

Lithosphere thickness (d) (km)	Crater radius (r_o) (km)	T_p 1450	h_o 0.15	η_o 10^{18}	Convective melt volume (km^3)	Convective melt duration (Ma)	Total melt volume (km^3)
		In situ melt volume (km^3)	Extant melt fraction	Maximum melt depth (km)			
50	50	3.7×10^4	0.81	118	3.3×10^3	9	1.9×10^5
	100	3.0×10^5	0.68	126	2.6×10^4	8	9.4×10^5
	200	2.6×10^6	0.49	142	8.0×10^4	6.5	5.1×10^6
	300	9.4×10^6	0.37	159	1.3×10^5	5.5	1.5×10^7
70	50	2.7×10^4	0.72	118	5.1×10^3	7	1.0×10^5
	100	2.2×10^5	0.56	126	1.4×10^4	5.5	5.1×10^5
	200	2.0×10^6	0.36	142	4.2×10^4	5.5	3.1×10^6
	300	7.4×10^6	0.25	159	1.0×10^5	5.5	1.0×10^7
100	50	1.1×10^4	0	118	0	0	1.1×10^4
	100	9.0×10^4	0	126	0	0	9.0×10^4
	200	9.3×10^5	0	142	0	0	9.3×10^5
	300	4.0×10^6	0	159	0	0	4.0×10^6
	400	1.2×0^7	0	175	0	0	1.2×10^7
150	300	9.2×10^5	0	159	0	0	9.2×10^5
	400	2.3×10^6	0	175	0	0	2.3×10^6

For stage 1, in situ decompression melting, some mantle potential temperatures are high enough that a melt fraction would exist beneath the lithosphere before impact. These conditions are considered unrealistic. The mantle background viscosity is used only in the numerical models for later convective melt. For a given lithospheric thickness, crater sizes that produce no melt are omitted from the table.

In any magmatic process, only a fraction of the magma produced will reach the surface. The largely basaltic melts predicted by these models are likely to have densities in the range 2800–3000 kg/m^3, while mantle peridotite is ~3300 kg/m^3, granitic crust ~2700 kg/m^3, and brecciated granite considerably less, perhaps as little as 1700 kg/m^3. Based simply on gravitational buoyancy, basalt liquids will not erupt through granite or breccia. Solidified melt sheets or fused material from lesser impact heat might form a cap against which rising magma would create a

pressure head sufficient to drive magma to the surface, and volatile content can also act as a driving force. Erupting magma faces the same force balances in any eruptive setting, and some fraction of the magma is certainly expected to remain beneath the surface.

3.2. Stage 2: adiabatic melting in convection currents

To test the hypothesis of convective melting under isostatically rebounded craters, we have run numerical experiments assuming lithospheric domes of varying heights formed under the crater. From the start of each of the numerical model runs, mantle material flows upward in the center of the dome and flows out and down at the edges. As convection continues, the strongest upward currents move toward the edges of the dome, and a countercirculating eddy outside the dome may form. Cooling thickens the lithosphere and convection currents are forced more deeply into the mantle. The strong downward-flowing limb of the cell at the rim of the dome may eventually pull from the edge of the dome material consisting of cool upper asthenosphere or the warmest lowest lithosphere. The lower the temperature

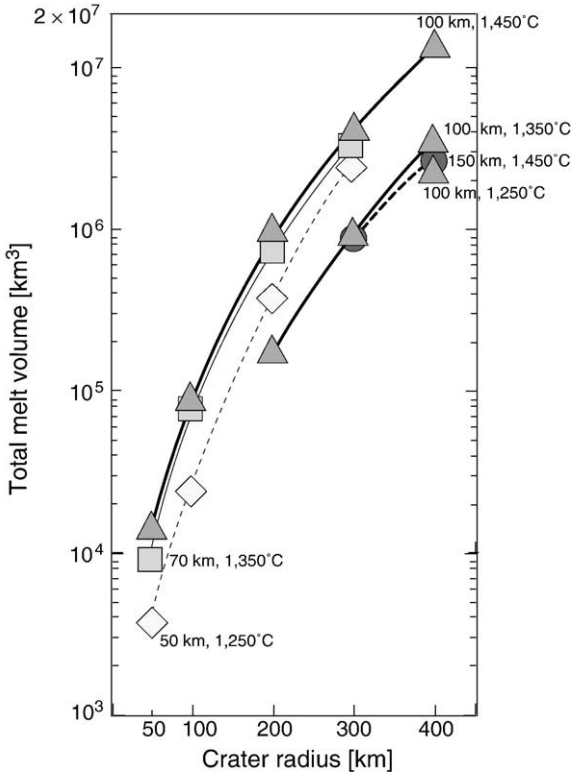

Fig. 4. Total melt volumes from impact as a function of crater excavation radius. Filled diamonds: 50-km lithospheres. Filled squares: 70-km lithospheres. Filled triangles: 100-km lithospheres. Mantle potential temperatures as marked.

Table 3
Effect on melt volume of varying lithospheric thickness, mantle potential temperature, and crater excavation depth

Effect of lithospheric thickness on melt volume				
	T_p	1250	1250	1250
	d	50 km	60 km	70 km
	h_o	0.15	0.15	0.15
r_o	50	3.6×10^3	0	0
	100	2.6×10^4	2.1×10^4	0
	200	3.9×10^5	2.0×10^5	1.5×10^5
	300	2.1×10^6	1.3×10^6	7.8×10^5
Effect of mantle potential temperature on melt volume				
	T_p	1250	1300	1350
	d	70 km	70 km	70 km
	h_o	0.15	0.15	0.15
r_o	50	0	0	9.3×10^3
	100	0	2.1×10^4	7.6×10^4
	200	1.5×10^5	3.1×10^5	8.2×10^5
	300	7.8×10^5	1.8×10^6	3.6×10^6
Effect of crater excavation depth on melt volume				
	T_p	1350	1350	
	d	70 km	70 km	
	h_o	0.15	0.10	
r_o	50	9.3×10^3	7.0×10^3	
	100	7.6×10^4	4.8×10^4	
	200	8.2×10^5	4.5×10^5	
	300	3.6×10^6	1.8×10^6	

Mantle potential temperature has the greatest effect on melt volume; a 50 °C change in mantle potential temperature changes melt volume by a factor of 2 or 3.

dependence of viscosity used in the models, the more likely these Rayleigh–Taylor instabilities become. Flow and temperature fields for one such experiment are shown in Fig. 5, where migration of the upwelling and development of a gravitational instability can be seen.

Though in lunar models, the convective stage produces small volumes of melt over a long period of time, in terrestrial models, only the thinnest lithosphere with the hottest mantle produces convective melt [6]. In other models, convection proceeds but fails to bring material to depths shallow enough to produce melt. The models demonstrate that even in the ideal case of maximum dome formation, very little or no melt is produced in the resulting convection cells for Earth.

4. Discussion

There is no unequivocal evidence that any flood-basalt province on Earth has been caused by a giant impact. The parameters of the models discussed in this

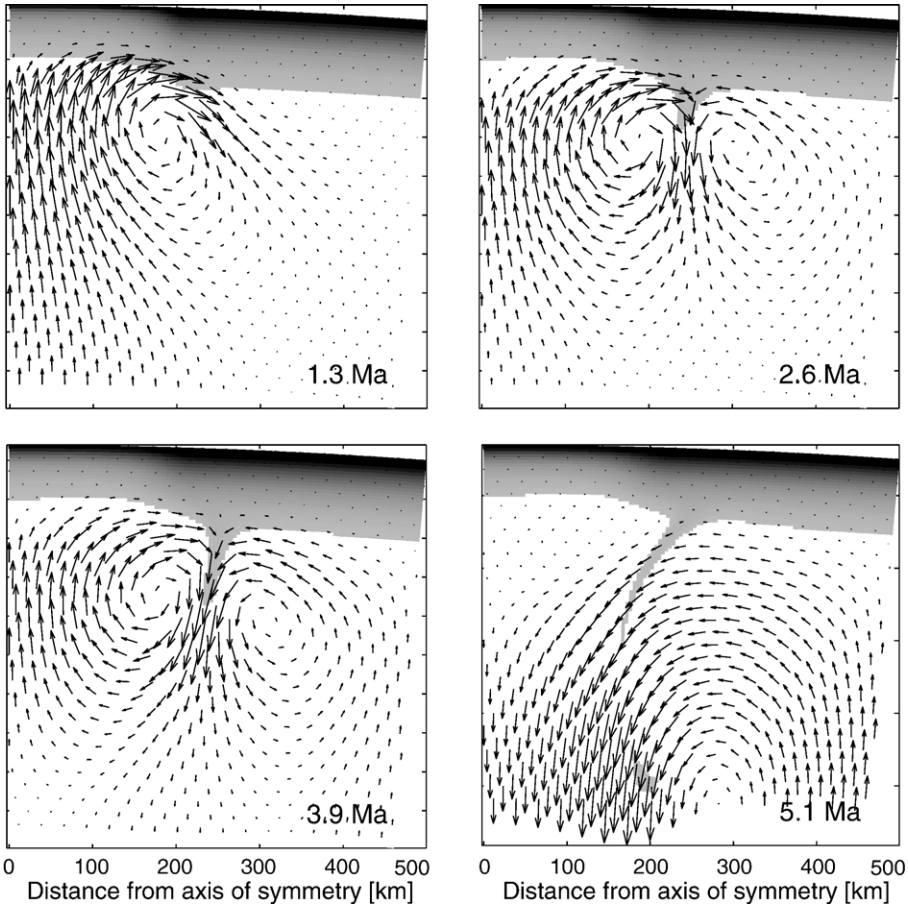

Fig. 5. Evolution of the mantle flow field in a numerical experiment with lithospheric thickness 70 km, crater excavation radius 200 km, activation energy for the temperature dependence of viscosity of ~400 kJ/mol, reference viscosity of 10^{18} Pa s, and square model box with scaled dimensions 500 × 500 km. Vectors indicate mantle flow and shading indicates temperature.

paper, however, are consistent with terrestrial conditions. Though Ivanov and Melosh [14] contend that impacts do not cause significant uplift of underlying strata, the melt that results in their numerical experiments is not significantly different from what we model here. We also contend that topography created by the impact at the rheological boundary between the lithosphere and asthenosphere may not be adequately modeled in the hydrocode simulations used, and we suggest that the domes in the lithosphere like those seen under craters on the moon may well be created by giant impacts on Earth.

We agree with Ivanov and Melosh [14] that craters with radii of 150 km and less cannot create melt except when made in the thinnest of lithospheres. Our models differ in scale: this suite of numerical models includes very large impacts and hotter mantle potential temperatures. We suggest that if an impact large enough to create the larger craters in this model occurred, the effects would be worldwide, and ample evidence could remain in the rock record.

As argon dating techniques have improved [49] and U–Pb dates obtained, the estimated durations of flood-basalt eruptions have shortened. The Siberian and Deccan flood basalts are thought to have occurred in 1 million yr or less [50,51], but others had longer durations. The Columbia flood basalts had a peak of eruption over about 1 million yr, but continued to erupt over 11 million yr [52]. The lingering volcanism is a result of the process of formation of the volcanic province and should be created by the model. A successful flood-basalt model, then, is required to create on the order of 10^6 km^3 of magma in less than 1 million yr. In the cases of the Siberian and Emeishan provinces, the model must allow subsidence during eruption and, in the case of the Columbia, produce lingering eruptions for about 10 Ma. Fig. 6 shows a comparison of melt volumes and eruption durations of flood-basalt provinces and model results. The models in which melt was only created by in situ depressurization produce all their magma in a very

brief time, and the volumes and durations fit the Siberian, Deccan, Emeishan, and Rajmahal provinces. Models in which later convection produces melt have longer durations of eruption and fit the Columbia flood basalts in volume and duration. These models therefore demonstrate the feasibility of a giant impact to cause flood basalt-sized eruptions in a geologically appropriate length of time.

The three largest known craters on Earth–Chicxulub, Sudbury, and Vredefort–do not have contemporaneous flood basalts associated with them. The Sudbury and Vredefort impactors both struck thick continental lithosphere and were relatively small compared to those modeled in this study: each had an estimated excavation radius of 50–70 km (scaling from [28,29], applied to data from [53]). Craters this size produce little or no mafic magma in lithospheres thicker than 75 km, according to our model results. Therefore, based on this study, we would expect no basaltic magmatism from either impact (though crustal melting from depressurization may have been significant in both cases and will be addressed elsewhere).

Chicxulub, the youngest and freshest of the large terrestrial impacts, had an excavation radius of about 50 km [42,43]. It struck a shallow ocean over the relatively thin lithosphere of a continental margin. Though the crater is the smallest size modeled in this study, if the lithosphere it struck was thin, Chicxulub would have been a reasonable candidate to create about 1000 km^3 of magma. There is, however, no known magmatism associated with Chicxulub. Deep seismic reflection studies carried out by Snyder et al. [54] show that there is no dome under Chicxulub. The shapes and positions of collapsed blocks and thrust faults under the crater indicate little or no fluid lithospheric flow during the initial cratering process. Their results, along with those of Pilkington et al. [42] and Morgan et al. [43], indicate that the cavity of Chicxulub is filled with breccia. We therefore agree with Ebbing et al. [27] that resurge must have nearly instantaneously filled Chic-

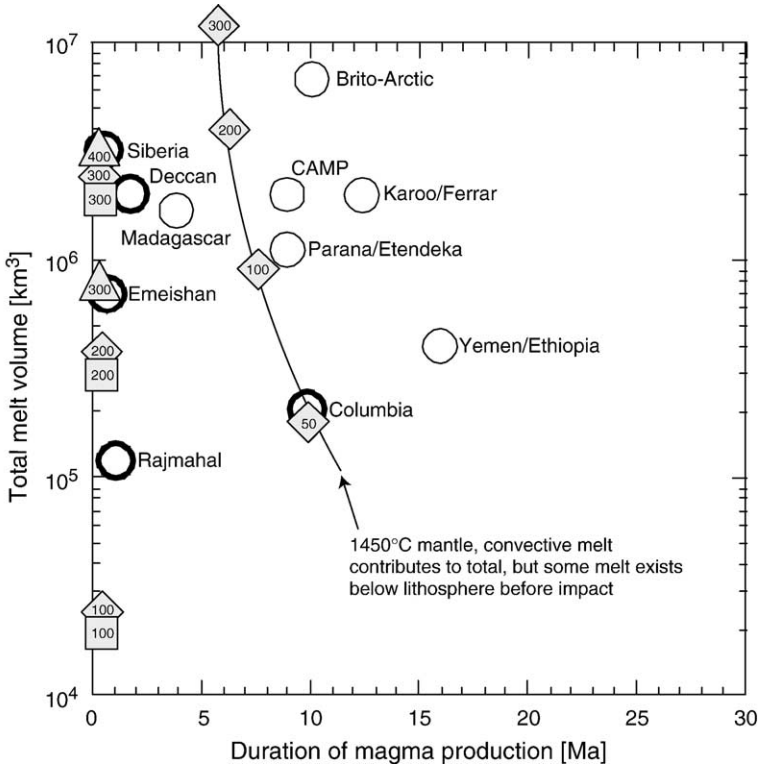

Fig. 6. Comparison of model results with terrestrial flood basalt provinces for the purposes of comparing volumes and durations of total melt production. Empty circles: terrestrial flood basalt provinces. Provinces that are not associated with complete rifting are outlined in black. Filled diamonds: models with 50-km lithosphere and either 1250 or 1450 °C mantle potential temperature. Filled squares: models with 70-km lithosphere and 1300 °C mantle potential temperature. Filled triangles: models with 100-km lithosphere and 1300 °C mantle potential temperature. Numbers in filled symbols denote crater excavation radii. References: Columbia: [52,55]. Yemen/Ethiopia: [56–59]. Brito-Arctic: [59–62]. Deccan: [51,56,63,64]. Madagascar: [65,66]. Rajmahal: [67,68]. Parana/Etendeka: [69–71]. Karoo/Ferrar: [72,73]. CAMP: [74–76]. Siberia: [50,77–80]. Emeishan: [81].

xulub with material, preventing in situ decompression melting and the formation of a lithospheric dome to force mantle convection.

5. Conclusions

A giant meteorite impact in thin lithosphere is a viable mechanism for creating a flood-basalt province on Earth. Mafic magma is produced by immediate in situ decompression and by later convective flow beneath a dome in the lithosphere–asthenosphere boundary that forms under the crater by instantaneous fluid flow of the lithosphere during impact and by later isostatic uplift. Volumes and durations of existing flood-basalt provinces are well fit by melt production in these models. Though there is no unequivocal evidence that giant impacts have created flood-basalt provinces on Earth, researchers continue to search for impact evidence coincident with flood-basalt formation. Basins of the age and size seen on the moon have been obliterated on the Earth through processes of plate tectonics and erosion, but the possibility remains of craters obscured beneath existing flood-basalt provinces. Magmatism from impact may have been additionally important in the early Archean when bombardment was more common and mantle potential temperatures may have been higher. The largest craters visible on Earth today–Chicxulub, Sudbury, and Vredefort–are not large enough to create flood basalts according to our model.

Acknowledgments

This work was supported by a National Defense Science and Engineering graduate fellowship and an Amelia Earhart graduate fellowship. The authors thank Walter Kiefer, Sue Smrekar, and Sean Solomon for thoughtful and constructive reviews, and Marc Parmentier for rewarding conversations on mechanisms of melting.

References

[1] L.W. Alvarez, W. Alvarez, F. Asaro, H.V. Michel, Extraterrestrial cause of the Cretaceous–Tertiary extinction, Science 208 (1980) 1008–1095.
[2] V.E. Courtillot, P.R. Renne, On the ages of flood basalt events, C. R. Géosci. 335 (2003) 113–140.
[3] D. Alt, J.M. Sears, D.W. Hyndman, Terrestrial maria: the origins of large basalt plateaus, hotspot tracks, and spreading ridges, J. Geol. 96 (1988) 647–662.
[4] D.H. Green, Archaean greenstone belts may include terrestrial equivalents of lunar maria? Earth Planet. Sci. Lett. 15 (1972) 263–270.
[5] D.H. Green, Petrogenesis of Archaean ultramafic magmas and implications for Archaean tectonics, in: A. Kroner (Ed.), Precambrian Plate Tectonics, Elsevier, Amsterdam, 1981, pp. 469–489.
[6] L.T. Elkins-Tanton, B.H. Hager, T.L. Grove, Magmatic effects of the lunar late heavy bombardment, Earth Planet. Sci. Lett. 222 (2004) 17–27.
[7] A.P. Jones, G.D. Price, N.J. Price, P.S. DeCarli, R.A. Clegg, Impact induced melting and development of large igneous provinces, Earth Planet. Sci. Lett. 202 (2002) 551–561.
[8] G. Ryder, Coincidence in time of the Imbrium basin impact and Apollo 15 KREEP volcanic flows: the case for impact-induced melting, in: B.O. Dressler, et al., (Eds.), Large Meteorite Impacts and Planetary Evolution, Special Paper-Geological Society of America, vol. 293, 1994, pp. 11–18.
[9] M.R. Rampino, Impact cratering and flood-basalt volcanism, Nature 327 (1987) 468.
[10] J.G. Negi, P.K. Agrawal, O.P. Pandey, A.P. Singh, A possible K–T boundary bolide impact site offshore near Bombay and triggering of rapid Deccan volcanism, Phys. Earth Planet. Inter. 76 (1993) 189–197.
[11] K. Kaihu, Y. Kajiwara, T. Nakano, Y. Miura, H. Kawahata, K. Tazaki, M. Ueshima, Z. Chen, G.R. Shi, End-Permian catrastrophe by a bolide impact: evidence of a gigantic release of sulfur from the mantle, Geology 29 (2001) 815–818.
[12] C.C. Reese, V.S. Solomatov, J.R. Baumbardner, D.R. Stegman, A.V. Vezolainen, Magmatic evolution of impact0induced Martian mantle plumes and the origin of Tharsis, J. Geophys. Res. 109 (2004), doi:10.1029/2003JE002222.
[13] H.J. Melosh, Can impacts induce volcanic eruptions? Abstract in Proceedings of "Catastrophic Events and Mass Extinction: Impacts and Beyond" Vienna, July 9–12, 2000.
[14] B.A. Ivanov, H.J. Melosh, Impacts do not initiate volcanic eruptions: eruptions close to the crater, Geology 31 (2003) 869–872.
[15] A.R. Basu, S. Chatterjee, D. Rudra, Shock-metamorphism in quartz grains at the base of the Deccan traps: evidence for impact-triggered flood basalt volcanism at the Cretaceous–Tertiary boundary, EOS Trans. 69 (1985) 1487.
[16] L. Becker, R.J. Poreda, A.G. Hunt, T.E. Bunch, M. Rapino, Impact event at the Permian–Triassic boundary: evidence from extraterrestrial noble gases in fullerines, Science 291 (2001) 1530–1533.
[17] D.-Y. Xu, S.L. Ma, Z.F. Chai, X.Y. Mao, Y.Y. Sun, Q.W. Zhang, Z.Z. Yang, Abundance variation of Iridium and trace elements at the Permian/Triassic boundary at Shangse in China, Nature 314 (1985) 154–156.
[18] C.J. Orth, M. Attrep, L.R. Quintana, Iridium abundance patterns across bio-event horizons in the fossil record, GSA Special Paper 247 (1990) 45–59.
[19] D.M. Bice, C.R. Newton, S. McCauley, P.W. Reiners, C.A. McRoberts, Shocked quartz at the Triassic–Jurassic boundary in Italy, Science 255 (1992) 443–446.
[20] M.R. Rampino, B.M. Haggerty, The "Shiva Hypothesis": impacts, mass extinctions, and the galaxy, Earth Moon, Planets 72 (1996) 441–460.
[21] R.A.F. Grieve, E.M. Shoemaker, The record of past impacts on earth, in: Tom Gehrels (Ed.), Hazards Due to Comets and Asteroids, U. of Arizona, 1994, pp. 417–462.
[22] T. Plank, C.H. Langmuir, Effects of the melting regime on the composition of the oceanic crust, J. Geophys. Res. 97 (1992) 19,749–19,770.

[23] R.J. Kinzler, T.L. Grove, Primary magmas of mid-ocean ridge basalts 1. Experiments and methods, J. Geophys. Res. 97 (1992) 6885–6906.
[24] D.C. Presnall, G. Gudfinnsson, M.J. Walter, Generation of mid-ocean ridge basalts at pressures from 1 to 7 GPa, Geochim. Cosmochim. Acta. 66 (2002) 2,073–2,090.
[25] D.H. Green, T. Falloon, S.M. Eggins, G.M. Yaxley, Primary magmas and mantle temperatures, Eur. J. Mineral. 13 (2001) 437–451.
[26] D.L. Anderson, T. Tanimoto, Y.-S. Zhang, Plate tectonics and hotspots: the third dimension, Science 256 (1992) 1645–1651.
[27] J. Ebbing, P. Janle, J. Koulouris, B. Milkereit, 3D gravity modelling of the Chicxulub impact structure, Planet. Space Sci. 49 (2001) 599–609.
[28] J.D. O'Keefe, T.J. Ahrens, Planetary cratering mechanics, J. Geophys. Res. 98 (1993) 17011–17028.
[29] J.D. O'Keefe, T.J. Ahrens, Complex craters: relationship of stratigraphy and rings to impact conditions, J. Geophys. Res. 104 (1999) 27,091–27,104.
[30] M.J. Cintala, R.A.F. Grieve, Scaling impact melting and crater dimensions: implications for the lunar cratering record, Meteorit. Planet. Sci. 33 (1998) 889–912.
[31] K.R. Housen, R.M. Schmidt, K.A. Holsapple, Crater ejecta scaling laws: fundamental forms based on dimensional analysis, J. Geophys. Res. 88 (1983) 2485–2499.
[32] H.J. Melosh, Impact Cratering: A Geological Process, Oxford University Press, Oxford, 1989, 245 pp.
[33] R.A.F. Grieve, M.J. Cintala, An analysis of differential impact-melt crater-scaling and implications for the terrestrial impact record, Meteoritics 27 (1992) 526–538.
[34] D. Steel, Distributions and moments of asteroid and comet impact speeds upon the Earth and Mars, Planet. Space Sci. 46 (1998) 473–478.
[35] E. Pierozzo, A.M. Vickery, H.J. Melosh, A reevalution of impact melt production, Icarus 127 (1997) 408–423.
[36] W.B. Tonks, H.J. Melosh, Magma ocean formation due to giant impacts, J. Geophys. Res. 98 (1993) 5319–5333.
[37] M.J. Walter, Melting of garnet peridotite and the origin of komatiite and depleted lithosphere, J. Pet. 39 (1998) 29–60.
[38] M.M. Hirschmann, Mantle solidus: experimental constraints and the effects of peridotite composition, Geochem. Geophys. Geosyst. 1 (2000).
[39] B.H. Hager, R.W. Clayton, in: W.R. Peltier (Ed.), Mantle Convection, Gordon and Breach, New York, 1989, pp. 657–763 (XX fix and complete this reference, if it is the one Brad wants).
[40] M.A. Wieczorek, R.J. Phillips, Lunar multiring basins and the cratering process, Icarus 139 (1999) 246–259.
[41] G.A. Neumann, M.T. Zuber, D.E. Smith, F.G. Lemoine, The lunar crust: global structure and signature of major basins, J. Geophys. Res. 101 (1996) 16,841–16,863.
[42] M. Pilkington, A.R. Hildebrand, C. Ortiz-Aleman, Gravity and magnetic field modeling and structure of the Chicxulub Crater, Mexico, J. Geophys. Res. 99 (1994) 13147–13162.
[43] J. Morgan, M. Warner, Chicxulub Working Group, Size and morphology of the Chicxulub impact crater, Nature 390 (1997) 472–476.
[44] H. Henkel, W.U. Reimold, Integrated geophysical modelling of a giant, complex impact structure: anatomy of the Vredefort Structure, South Africa, Tectonophysics 287 (1998) 1–20.
[45] V.A. Fedorenko, P.C. Lightfoot, A.J. Naldrett, G.K. Czamanske, C.J. Hawkesworth, J.L. Wooden, D.S. Ebel, Petrogenesis of the flood-basalt sequence at Noril'sk, North-central Siberia, Int. Geol. Rev. 38 (1996) 99–135.
[46] G.M. Thompson, J.R. Ali, X.Y. Song, D.W. Jolley, Emeishan basalts, SW China: reappraisal of the formation's type area stratigraphy and a discussion of its significance as a large igneous province, J. Geol. Soc. (Lond.) 158 (2001) 593–599.
[47] S.D. King, A. Raefsky, B.H. Hager, ConMan: vectorizing a finite element code for incompressible two-dimensional convection in the Earth's mantle, Phys. Earth Planet. Inter. 59 (1990) 195–207.
[48] D.L. Turcotte, G. Schubert, Geodynamics, Cambridge University Press, Cambridge, England, 2002, 456 pp.
[49] J. Baker, L. Snee, M.A. Menzies, A brief Oligocene period of volcanism in Yemen; implications for the duration and date of continental flood volcanism at the Afro-Arabian triple junction, Earth Planet. Sci. Lett. 138 (1996) 39–55.
[50] S.A. Bowring, D.H. Erwin, Y.G. Jin, M.W. Martin, K. Davidek, W. Wang, U–Pb zircon geochronology and the tempo of the end-Permian mass extinction, Science 280 (1998) 1039–1045.
[51] A.K. Baksi, Geochronological studies on whole-rock basalts, Deccan Traps, India: evaluation of the timing of volcanism relative to the K–T boundary, Earth Planet. Sci. Lett. 121 (1994) 43–56.
[52] P.R. Hooper, C.J. Hawkesworth, Isotopic and geochemical constraints on the origin abd evolution of the Columbia River Basalt, J. Pet. 34 (1993) 1203–1246.
[53] R.A.F. Grieve, A. Therriault, Vredefort, Sudbury, Chicxulub: three of a kind? Annu. Rev. Earth Planet. Sci. 28 (2000) 305–338.
[54] D.B. Snyder, R.W. Hobbs, Chicxulub Working Group, Ringed structural zones with deep roots formed by the Chicxulub impact, J. Geophys. Res. 104 (1999) 10743–10755.
[55] P.R. Hooper, The Columbia River flood basalt province: current status, in: J.D. Macdougall (Ed.), Continental Flood Basalts, Kluwer, 1997, pp. 1–27.
[56] T.R. Venkatasan, K. Pande, K. Gopalan, Did Deccan volcanism pre-date the Cretaceous/Tertiary transition? Earth Planet. Sci. Lett. 119 (1993) 181–189.
[57] V. Zumbo, G. Feraud, H. Bertrand, G. Chazot, $^{40}Ar/^{39}Ar$ chronology of the Tertiary magmatic activity in Southern Yemen during the early Red Sea–Aden rifting, J. Volcanol. Geotherm. Res. 65 (1995) 265–279.
[58] T. Chernet, W.K. Hart, J.L. Aronson, R.V. Walter, New age constraints on the timing and tectonism in the northern Main Ethiopian Rift–southern Afar transition zone (Ethiopia), J. Volcanol. Geotherm. Res. 80 (1998) 267–280.
[59] A.E. Mussett, $^{40}Ar/^{39}Ar$ step heating ages of the Tertiary igneous rocks of Mull, Scotland, J. Geol. Soc. (Lond.) 143 (1986) 887–896.
[60] I.G. Meighan, A.G. McCormick, D. Gibson, J.A. Gamble, I.J. Graham, Rb–Sr isotopic determinations and the timing of Tertiary central complex magmatism in Northeast Ireland, in: A.C. Morton, L.M. Parson (Eds.), Early Tertiary Volcanism and the Opening of the Northeastern Atlantic, Special Publication-Geological Society of London, vol. 39, 1988, pp. 349–360.
[61] B.G.J. Upton, C.H. Emeleus, D.C. Rex, M.F. Thirlwall, Early Tertiary magmatism in Northeast Greenland, J. Geol. Soc. (Lond.) 152 (1995) 959–964.
[62] D.G. Pearson, C.H. Emeleus, S.P. Kelley, Precise $^{40}Ar/^{39}Ar$ age for the initiation of Paleogene volcanism in the Inner Hebrides and its regional significance, J. Geol. Soc. (Lond.) 153 (1996) 815–818.

[63] V. Courtillot, Deccan volcanism at the Cretaceous–Tertiary boundary: past climatic crises as a key to the future? Palaeo^3 189 (1990) 291–299.
[64] J.S. Ray, K. Pande, Carbonatite alkaline magmatism associated with continental flood basalts at stratigraphic boundaries: cause for mass extinctions, Geophys. Res. Lett. 26 (1999) 1917–1920.
[65] M. Storey, J.J. Mahoney, A.D. Saunders, R.A. Duncan, S.P. Kelley, M.F. Coffin, Timing of hot spot-related volcanism and the breakup of Madagascar and India, Science 267 (1995) 852–855.
[66] T.H. Torsvik, R.D. Tucker, L.D. Ashwal, E.A. Eide, N.A. Rakotosolofo, M.J. de Wit, Late Cretaceous magmatism in Madagascar: paleomagnetic evidence for a stationary Marion hot spot, Earth Planet. Sci. Lett. 164 (1998) 221–232.
[67] M.S. Pringle, ^{40}Ar/^{39}Ar geochronology of Mid-Cretaceous Indian Ocean basalts: constraints on the origin of large flood basalt provinces, AGU Fall Meeting Abstract V32A-13, 1994, p. 728.
[68] A.K. Baksi, Petrogenesis and timing of volcanism in the Rajmahal flood basalt province, northeastern India, Chem. Geol. 121 (1995) 73–90.
[69] S. Turner, M. Regelous, S. Kelley, C. Hawkesworth, M. Mantovi, Magmatism and continental breakup in the south Atlantic: high precision ^{40}Ar/^{39}Ar geochronology, Earth Planet. Sci. Lett. 121 (1994) 333–348.
[70] K. Stewart, S. Turner, S. Kelly, C. Hawkesworth, L. Kirstein, M. Mantovani, 3-D ^{40}Ar–^{39}Ar geochronology in the Parana continetnal flood basalt province, Earth Planet. Sci. Lett. 143 (1996) 95–109.
[71] P.R. Renne, J.M. Glen, S.C. Milner, A.R. Duncan, Age of Etendeka flood volcanism and associated intrusions in southwestern Africa, Geology 24 (1996) 659–662.
[72] D.R. Minor, S.B. Mukasa, Zircon U–Pb and hornblende ^{40}Ar–^{39}Ar ages for the Dufek layered mafic intrusion, Antarctica: implications for the age of the Ferrar large igneous province, Geochim. Cosmochim. Acta 61 (1997) 2497–2504.
[73] R.A. Duncan, P.R. Hooper, J. Rehacek, J.S. Marsh, A.R. Duncan, The timing and duration of the Karoo igneous event, southern Gondwana, J. Geophys. Res. 102 (1997) 18127–18138.
[74] K. Deckart, G. Feraud, H. Bertrand, Age of Jurassic continental tholeiites of French Guyana, Surinam and Guinea: implications for the initial opening of the Central Atlantic Ocean, Earth Planet. Sci. Lett. 150 (1997) 205–220.
[75] A. Marzoli, P.R. Renne, E.M. Piccirillo, M. Ernesto, G. Bellieni, A. De Min, Extensive 200-million-year-old continental flood basalts of the Central Atlantic Magmatic Province, Science 284 (2000) 616–618.
[76] W.E. Hames, P.R. Renne, C. Ruppel, New evidence for geologically instantaneous emplacement of earliest Jurassic Central Atlantic magmatic province basalts on the North American margin, Geology 28 (2000) 859–862.
[77] P.R. Renne, A.R. Basu, Rapid eruption of the Siberian Traps flood basalts at the Permo-Triassic boundary, Science 253 (1991) 176–179.
[78] P.R. Renne, Excess ^{40}Ar in biotite and hornblende from the Noril'sk 1 intrusion, Siberia: implications for the age of the Siberian Traps, Earth Planet. Sci. Lett. 131 (1995) 165–176.
[79] P.R. Renne, Z. Zichao, M.A. Richards, M.T. Black, A.R. Basu, Synchrony and causal relations between Permian–Triassic boundary crises and Siberian flood volcanism, Science 253 (1995) 1413–1416.
[80] S.L. Kamo, G.K. Czamanske, T.E. Krough, A minimum U–Pb age for Siberian flood basalt volcanism, Geochim. Cosmochim. Acta 60 (1996) 3505–3511.
[81] M.I. Zhou, J. Milpas, X.Y. Song, P.T. Robinson, A.K. Kennedy, M. Sun, G. Thompson, D. Yan, C.J. Zhong, SHRIMP zircon geochronology of the Emeishan large igneous province (SW China): implications for double mass extinctions in the late Permian, 11th Goldschmidt Conference, Virginia, Abstract #3519, 2001.